



HAL
open science

Customizable and Reconfigurable Surface Properties of Printed Micro-objects by 3D Direct Laser Writing via Nitroxide Mediated Photopolymerization

Mehdi Belqat, Xingyu Wu, Jason Morris, Karine Mougín, Tatiana Petithory, Laurent Pieuchot, Yohann Guillaneuf, Didier Gigmes, Jean-louis Clément, Arnaud Spangenberg

► To cite this version:

Mehdi Belqat, Xingyu Wu, Jason Morris, Karine Mougín, Tatiana Petithory, et al.. Customizable and Reconfigurable Surface Properties of Printed Micro-objects by 3D Direct Laser Writing via Nitroxide Mediated Photopolymerization. *Advanced Functional Materials*, 2023, 33 (39), 10.1002/adfm.202211971 . hal-04274320

HAL Id: hal-04274320

<https://cnrs.hal.science/hal-04274320>

Submitted on 7 Nov 2023

HAL is a multi-disciplinary open access archive for the deposit and dissemination of scientific research documents, whether they are published or not. The documents may come from teaching and research institutions in France or abroad, or from public or private research centers.

L'archive ouverte pluridisciplinaire **HAL**, est destinée au dépôt et à la diffusion de documents scientifiques de niveau recherche, publiés ou non, émanant des établissements d'enseignement et de recherche français ou étrangers, des laboratoires publics ou privés.

Customizable and Reconfigurable Surface Properties of Printed Micro-objects by 3D Direct Laser Writing via Nitroxide Mediated Photopolymerization

Mehdi Belqat, Xingyu Wu, Jason Morris, Karine Mougín, Tatiana Petithory, Laurent Pieuchot, Yohann Guillaneuf, Didier Gigmes, Jean-Louis Clément, and Arnaud Spangenberg*

Photoactivated Reversible Deactivation Radical Polymerization (RDRP) technologies have emerged very recently in the field of 3D printing systems especially at the macroscale in vat-photopolymerization-based processes such as digital light processing (DLP). Contrary to conventional free radical photopolymerization, photoRDRP in 3D printing leads to 3D objects with living character and thus confers them the unique ability to be post-modified after fabrication. While 3D direct laser writing (3D DLW) by two photon polymerization has become a standard for fabrication of complex 3D micro-objects, the use of RDRP and its associated benefits has so far been under-investigated at that scale. Herein, a photoresist suitable for 3D DLW based on nitroxide mediated photopolymerization (NMP2) is developed. The photopolymerization efficiency for fabrication of micro-structures and their subsequent post-modification are investigated regarding the laser power and the wavelength of excitation. Moreover, highly tunable, precise, and successive surface patterning of 2D and 3D multi-material microstructures are demonstrated thanks to the spatial and temporal control offered by the photo-induced post-modification. This work highlights new directions to be explored in order to accelerate the adoption of RDRP in 3D printing based on photopolymerization.

ization-based 3D printing in particular at the macroscale by using digital light processing (DLP) techniques.^[1] Indeed, in conventional free radical photopolymerization, a heterogeneous polymer network of “dead” chains is formed due to irreversible termination reactions. In contrast, in RDRP the “living” character of the polymer network is ensured via the presence of dormant reactivable polymer chains, resulting in the formation of more homogeneous polymer network. Besides, the ability to reversibly deactivate chain growth provides additional appealing features to the synthesized polymer network such as its reprocessability, both from chemical or mechanical point of view.^[2]

As an extension of the exciting opportunities opened in polymer network formation, various photoRDRP strategies have been applied to 3D printing with the aim to enable the elaboration of 3D objects with customizable and reconfigurable properties.^[1b]

In that regard, pioneering work was carried out by Bagheri et al. with the employ of photoiniferter reversible activation fragmentation chain transfer (RAFT) polymerization in DLP 3D printing under a nitrogen environment.^[1a] The direct photolysis under visible light irradiation of trithiocarbonate RAFT agent allows to fabricate 3D objects with living character. The latter was demonstrated via the post-modification of surface properties with fluorescent monomers. In order to improve the printing speed and make compatible photoRDRP with open-air DLP 3D printers, Boyer and co-workers have successfully proposed an alternative strategy namely photoinduced electron/energy transfer-RAFT (PET-RAFT) polymerization.^[1d] The employ of an organic dye (photocatalyst), a tertiary amine (co-catalyst), a RAFT agent, and acrylate monomers allowed faster printing and photo-induced post-modification of 3D printed objects. In a subsequent study, Bagheri et al. also reported the first examples of oxygen tolerant PET-RAFT formulation for fully open to air 3D printing.^[3] Since then, more sophisticated systems were developed using either a combination of cationic and radical based RAFT polymerization,^[4] the use of RAFT-capable TTC crosslinkers^[5] or targeting the preparation of highly resolved micro- and macroscale features.^[6] More recently

1. Introduction

Recently, Reversible Deactivation Radical Polymerization (RDRP) has drawn tremendous attention in photopolymer-

M. Belqat, X. Wu, K. Mougín, T. Petithory, L. Pieuchot, A. Spangenberg
Université de Haute-Alsace
CNRS

IS2M UMR 7361, Mulhouse F-68100, France
E-mail: arnaud.spangenberg@uha.fr

M. Belqat, X. Wu, K. Mougín, T. Petithory, L. Pieuchot, A. Spangenberg
Université de Strasbourg
Strasbourg, France

J. Morris, Y. Guillaneuf, D. Gigmes, J.-L. Clément
Aix Marseille University
CNRS, ICR UMR7273, Marseille F-13397, France

 The ORCID identification number(s) for the author(s) of this article can be found under <https://doi.org/10.1002/adfm.202211971>.

© 2023 The Authors. Advanced Functional Materials published by Wiley-VCH GmbH. This is an open access article under the terms of the Creative Commons Attribution License, which permits use, distribution and reproduction in any medium, provided the original work is properly cited.

DOI: 10.1002/adfm.202211971

photoRDRP has been also extended to photoATRP by Qiao et al.^[1f] and Boyer's group has developed Norrish type I photo-initiated RAFT polymerization (NTI-RAFT).^[1c] In the latter example, rapid high-resolution 3D printing capability is highlighted and impressive spatial control of the post-modification is demonstrated. This work confirms the positive role played by RAFT agent to improve the resolution as described early by Guymon's group.^[1e]

Interestingly, up to now, application of photoRDRP techniques have been mainly limited to DLP 3D printing. Exploiting these approaches in the field of 3D direct laser writing (3D DLW) based on two-photon polymerization^[7] will undeniably open new perspectives in the production of multi-functional 3D microstructures that are highly desired for various applications, including soft robotics,^[8] or tissue engineering^[7a,9] to quote a few. The numerous efforts currently devoted to control the surface properties of such 3D microstructures highlight the importance to develop alternative strategies facilitating the customization and reconfiguration of the printed micro-objects.^[8c,10]

Surprisingly, the employ of photoRDRP in 3D DLW and its associated benefits, including tunability of surface and bulk properties, have been so far under-investigated.

Pioneered by our group,^[11] implementation of photoRDRP in 3D DLW has been recently demonstrated via photo-induced reactivation of macro-photoiniferter RAFT polymerization. Spatial control of the photo-induced post-modification has been highlighted by writing the letters "μRAFT" and by patterning thermo-responsive functional material on the printed surface. Very recently, Blasco et al. have proposed a new approach for the preparation of covalent adaptable microstructures by 3D DLW. This approach lies in the inclusion of an alkoxyamine in the formulation allowing for chain extension via nitroxide mediated polymerization (NMP).^[12] This approach has led to impressive volume change and tunability of the mechanical properties by two orders of magnitude of the printed micro-object induced by thermal post-modification. However, photo-induced post-modification has not been attempted limiting the possibility to introduce multiple functionalities in a spatial control manner. These two recent examples underline the interest to further investigate photoRDRP in 3D DLW that enable the fabrication of 3D micro-objects with adaptable and reconfigurable properties. Following our previous work on photoiniferter,^[11] we moved towards another photo-RDRP technique that is also based on an intramolecular photo-initiation mechanism: the Nitroxide-Mediated PhotoPolymerization (NMP2). We pioneered this field in 2010 by introducing a chromophore on an alkoxyamine to convert thermal dissociation into photochemical dissociation that allow us to developed the so called Nitroxide-Mediated PhotoPolymerization (NMP2).^[13] This technique was then used to prepare reactivable micropatterns.^[14] We already demonstrated that reactivable micropatterns could be obtained via the combination of NMP2 and direct laser writing using laser diode emitting at 375 nm.^[15] In the current work, due to the mechanism of multiphoton absorption that required to occur in a very small volume, RDRP systems that are based on an intramolecular activation are preferred. The use of NMP2 in that application is very interesting since very high rate of polymerization has been reported for such system

and their efficient use in micropatterning led us confident to obtain a high degree of reinitiation.

Herein, a solvent free photoresist suitable for 3D DLW based on nitroxide mediated photopolymerization (NMP2) is developed. The photopolymerization efficiency for fabrication of micro-structures and their subsequent post-modification are investigated regarding the laser power and the wavelength of excitation. Moreover, highly tunable, precise, and successive surface patterning of 2D and 3D multi-material microstructures are demonstrated thanks to the spatial and temporal control offered by the photo-induced post-modification. This work highlights new directions to be explored in order to accelerate the adoption of RDRP in 3D DLW and more broadly in 3D printing based on photopolymerization.

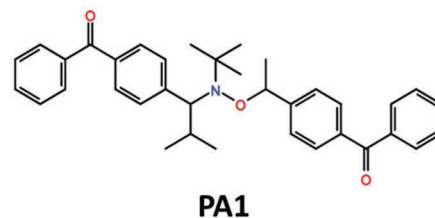
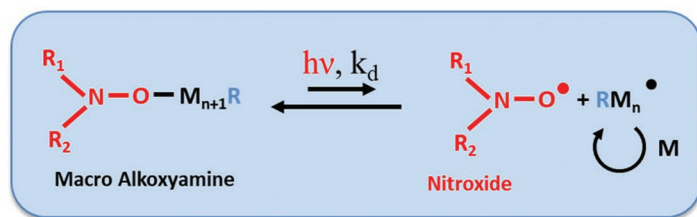
2. Results and Discussion

2.1. Investigating Two-Photon Polymerization Properties of Alkoxyamine PA1-Based Resin

2.1.1. Mechanism of NMP2 and Selection of Alkoxyamine PA1 for NMP2 3D DLW

As depicted in **Figure 1a**, under light excitation, the alkoxyamines bearing benzophenone groups can undergo homolysis of the C–O bond without catalyst or external additive to generate a carbon radical ($R\cdot$) and a stable nitroxide radical ($\cdot O-NR_1R_2$). The $R\cdot$ species undergoes further propagation in the presence of monomers. During chain growth, the polymer radical $R-P_n\cdot$ is reversibly terminated by the persistent radical $\cdot O-NR_1R_2$ to produce the dormant species $R-P_n-ONR_1R_2$, thus providing a means of controlling the radical polymerization process. Similar to $R-O-NR_1R_2$, the resulting macro-alkoxyamine, i.e., the dormant species, can also undergo reversible initiation under light conditions, which facilitates further propagation. Several alkoxyamines bearing one or two benzophenone derivatives have already been studied by our working group.^[13–14] The C–O bond cleavage has been demonstrated and for some of them the photolysis rate constants (k_d) were determined over a large range of light intensity via the monitoring of the nitroxide concentration in aerated conditions.^[13b] Besides, some of them have been used successfully for micropatterning with a detailed study of their photoinitiation efficiencies.^[14–16] The nitroxide used was already described elsewhere^[14b] and was designed to improve its stability by the introduction of an isopropyl group that impede the disproportionation that could occur when a methyl moiety is present.^[17] Second, a second benzophenone moiety was also inserted into the alkyl fragment of the alkoxyamine in PA1 since we showed that such alkyl group increased the rate of photolysis and thus will impart a better photoinitiation.^[16] The fast and selective cleavage of the alkoxyamine was qualitatively observed by ESR (See Figure S1, Supporting Information) and its photoinitiation ability was compared to BAPO, a commercial photoinitiator, by performing in situ FTIR experiments (see Figure S2, Supporting Information). One can notice that the photopolymerization rate initiated by PA1 is slower, but the novelty brought by PA1 lies in the living properties of polymer chains after photopolymerization, which has

a) Nitroxide Mediated PhotoPolymerization (NMP2)



b) Two-photon Induced NMP2 for Fabrication (λ_1, P_1) and Functionalization (λ_2, P_2)



c) Investigation of impact of laser power (P_1, P_2) and wavelength (λ_1, λ_2)

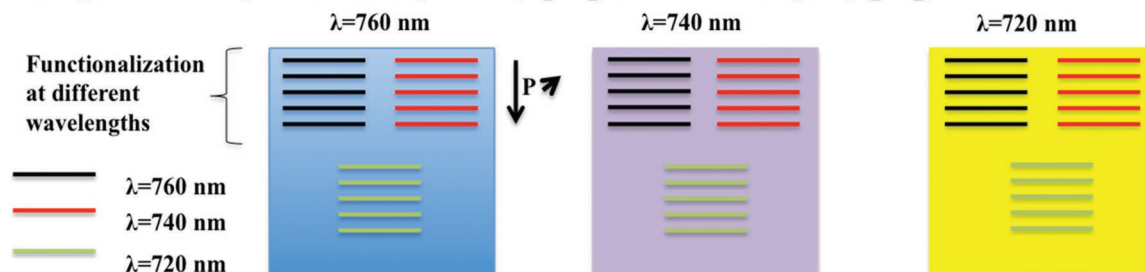


Figure 1. a) Overview of the NMP2 polymerization mechanism involving a reversible photolysis, and molecular structure of the alkoxyamine PA1 used in this work. b) Schematic representation of the fabrication (Step 1) and functionalization (Step 2) both made by 3D direct laser writing via nitroxide mediated photopolymerization reaction. c) Optimizing of writing parameters (wavelength and laser power) for fabrication and functionalization steps.

been exploited in surface modification presented in this work. Herein, a typical solvent-free formulation contains pentaerythritol triacrylate (PETA, see Figure S3, Supporting Information) as a monomer and crosslinker, and the alkoxyamine PA1 (3 wt.%) as photoinitiator and precursor of macroalkoxyamine. PA1's synthesis is described in Section S4 (Supporting Information). It has to be noted that the incorporation of benzophenone derivative within alkoxyamine unit is expected to provide the ability to perform two-photon induced NMP2 both for fabrication and functionalization.

2.1.2. Two-Photon Polymerization Efficiency of PA1

The evaluation of the efficiency of a photoinitiator in 3D DLW usually comes down to determining the two-photon cross section δ and the radical generation quantum yield Φ . However, it has to be mentioned that the determination of both values depends on the methods used and the experimental conditions

(nature of solvent, presence of oxygen, concentration...). Thus, it may not reflect the experimental conditions encountered during a two-photon photopolymerization. Therefore, in the current study, the performance of PA1 to induce two-photon polymerization has been probed according to the formalism proposed by Baldacchini et al.^[18] where the threshold power is related to the product $\delta \cdot \Phi$ such as:

$$\frac{1}{P_{th}^2} = \delta \cdot \Phi \cdot k \quad (1)$$

With k a constant taking into account the fixed experimental parameters (numerical aperture of the microscope). Experimentally, the two-photon polymerization threshold power (P_{th}) is determined at a given wavelength by polymerizing lines with decreasing power (Figure 1b, fabrication step). Microstructures were formed by focusing the femtosecond laser beam into a drop of PETA/PA1 resin using a 40 \times magnification objective with writing speed fixed at 14.3 $\mu\text{m s}^{-1}$. When the power is not

sufficient to induce the formation of polymerized lines, the threshold value is obtained. According to Equation 1, the relative values of the two-photon polymerization action spectrum of PA1 in PETA can be derived from the plot of $1/P_{th}^2$ versus the excitation wavelength from 710 to 800 nm. The threshold power being inversely proportional to the product $\Phi \cdot \delta$: the higher this value, the lower the laser power required to initiate the polymerization, which consequently reflects a better sensitivity of the photoinitiating system. Thus, at 710 nm, it can be assumed that the generation of radicals via PA1 is the most important. Stable PETA-based microstructures could be obtained between 710 and 760 nm in the presence of oxygen. For wavelengths above 760 nm, the photopolymerization reaction is initiated, but not sufficiently advanced to withstand the development stage.

2.1.3. Living Character of NMP2 Printed Microstructures

Having established the ability of PA1 to initiate microstructuration via two-photon polymerization, we aim to highlight the living character of the resulting microstructure. For this proof of concept, the fabrication (λ_1) and functionalization (λ_2) excitation wavelengths are set both at 720 nm, where PA1 exhibits higher initiating efficiency and where our tunable excitation laser source presents better mode locking (stability) and higher energy necessary for investigating the impact of laser power (see next section). First, a drop of the resin is deposited in a glass coverslip. Then, the laser beam is focused into the drop to induce the two-photon polymerization of a squared microstructure at a laser power $P_1 = 3.84$ mW close to the threshold energy in presence of oxygen. Finally, the microstructure is obtained after a development step in ethanol (Figure 1b – Fabrication step). For functionalization experiment, a drop of trimethylolpropane triacrylate (TMPTA, see Figure S3, Supporting Information) resin without photoinitiator is deposited on the top of the fabricated squared structure. The laser beam is focused on the upper surface of the already formed microstructure (Figure 1b, Functionalization step). In the presence of oxygen, no functionalization could be evidenced. The experiment was therefore carried out under a controlled atmosphere (nitrogen). In this case, lines of TMPTA were produced with a laser power

P_2 ranging from 3.84 to 8.4 mW. The heights Δh of repolymerized lines were measured by Atomic Force Microscopy (AFM) and plotted in function of laser power P_2 (Figure 2b). The AFM image of these lines and associated profile are given in Figure S4 (Supporting Information). The results obtained evidenced an increase in the line's height Δh as a function of the laser power P_2 . These results therefore highlight the living and controlled nature of the reaction. It has to be noted that in the context of microstructuring, the living character is defined by the possibility of re-initiating a polymerization without additional contribution of a photoinitiator. The controlled character is attributed to the possibility of precisely varying the geometry (Δh) of the repolymerized lines according to a given parameter, here the power. Indeed, by increasing the power of the laser, the heights of the repolymerized lines increase linearly from 267 to 554 nm.

2.2. Optimizing Writing Parameters for Fabrication and Functionalization via NMP2

Having established the living character of microstructures made by NMP2 3D DLW, we implemented similar methodology described in Section 2.1.3 to investigate the impact of laser power and excitation's wavelength both for fabrication and functionalization steps (Figure 1c). Our motivation to investigate the influence of laser power is driven by previous works of our consortium focused on NMP2. For instance, Versace et al. reported that the photolysis rate constants k_d of the alkoxyamines can be modulated by varying light intensity. More recently, in the context of UV patterning, the power of the excitation source was found to be a key parameter to tune the extent of the repolymerization.^[14b,16] One can reasonably assume that the extent of the repolymerization should be related to the production of reactive species at a given time and in a given volume. Therefore, according to the wavelength dependency shown by PA1 for two-photon polymerization and according to recent results focused on wavelength-resolved ATRP obtained by Nardi et al. in solution,^[19] we decided to investigate for the first time the influence of the excitation's wavelength on NMP2 3D DLW.

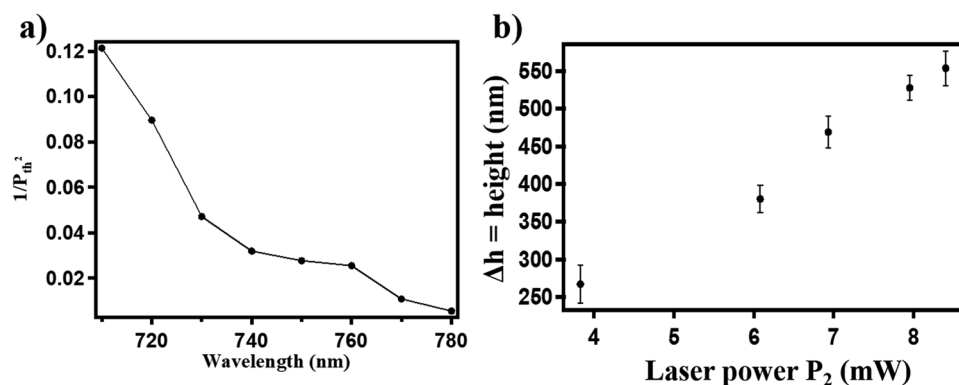


Figure 2. a) Two-photon absorption (TPA) action polymerization spectrum of PETA based formulation containing PA1 (3 wt.%). b) Validation of the living character of the printed $30 \times 30 \mu\text{m}^2$ square by 3D DLW at $\lambda_1 = 720$ nm ($P_1 = 3.84$ mW), and functionalization by NMP2 at $\lambda_2 = 720$ nm of several lines with increasing power P_2 from 3.84 to 8.4 mW.

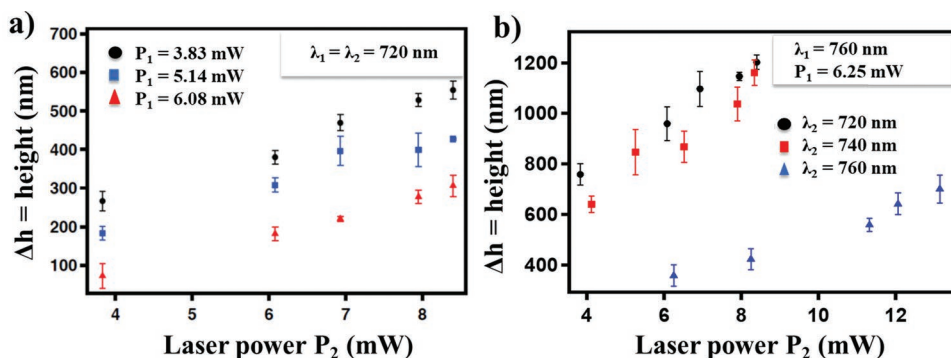


Figure 3. a) Influence of laser power P_1 and P_2 on the extent of the repolymerization by NMP2. The excitation wavelengths for fabrication and functionalization are fixed and set at 720 nm. Laser power P_1 for fabrication is set to 3.83, 5.14, or 6.08 mW. For each P_1 , laser power P_2 is modulated between 3.83 and 8.4 mW. b) Influence of functionalization excitation wavelength λ_2 on the extent of the repolymerization by NMP2 for different laser power P_2 . Laser power P_1 for fabrication is set to 6.25 mW, and laser power P_2 is modulated to a certain range specific to each λ_2 . The excitation wavelength for fabrication is fixed at $\lambda_1 = 760$ nm.

2.2.1. Laser Power Mediated Surface Modification

For sake of clarity, only the data obtained with excitation wavelengths fixed at $\lambda_1 = \lambda_2 = 720$ nm are discussed. The set of data related to excitation wavelengths fixed at $\lambda_1 = \lambda_2 = 740$ nm or at $\lambda_1 = \lambda_2 = 760$ nm are added in Sections S6 (Figure S5 and Table S1, Supporting Information) and S7 (Figure S6 and Table S2, Supporting Information) respectively.

As already discussed in Section 2.1.3, the extent of polymerization during a post-modification of square microstructures is favored with increasing laser power P_2 . As depicted in Figure 3a, similar trends are observed whatever the laser power used (P_1) for the fabrication of squares. However the height of the repolymerized lines are slightly different for laser power P_1 ranging from 3.83 to 6.08 mW. Indeed, while for P_1 set to 3.83 mW the height is varying from 267 to 554 nm, when P_1 is set to 5.14 mW or 6.08 mW, the height is varying from 184 to 427 nm or from 73 to 306 nm, respectively. Interestingly, the living character of the structures is confirmed for any printing conditions, and these results demonstrate our ability to finely tune the extent of the repolymerization from 73 nm up to 554 nm by adjusting the fabrication laser power P_1 (Table 1). One can also notice that for a given functionalization laser power P_2 , the repolymerized height is decreasing when the laser power P_1 is increasing. One can assume that at higher laser power P_1 , the degree of reticulation of the polymer network is more pronounced thus limiting the interpenetration between the macro-alkoxyamine formed during the fabrication step, and the new monomer added during the functionalization step.

2.2.2. Wavelength Dependence of the Functionalization

In order to study the influence of wavelength on the functionalization, several groups of lines made from TMPTA alone using different wavelengths were fabricated on a square ($20 \mu\text{m} \times 20 \mu\text{m}$) made from PETA/PA1 with a fixed wavelength and laser power. As shown in Figure 3b, the bottom square was made at $\lambda_1 = 760$ nm, $P_1 = 6.25$ mW, and on the square, three different wavelengths ($\lambda_2 = 720, 740,$ and 760 nm) were applied for functionalization. From the plot of the lines' heights (Δh), measured from AFM, against laser power (P_2), we can clearly see the increase of heights Δh with the laser power (P_2) increasing at each wavelength (λ_2), as discussed above. Focusing on the wavelength, it is evidenced that at the same laser power (P_2), with longer wavelength (λ_2), the heights of lines Δh are smaller. For example, at $P_2 = 8.25$ mW, the Δh of a line made at $\lambda_2 = 720$ nm is 1203 nm. This value of Δh decreases to 1161 nm at $\lambda_2 = 740$ nm, and further to 423 nm at $\lambda_2 = 760$ nm. This is not only valid for functionalization on a square made at $\lambda_1 = 760$ nm, functionalization on squares made at $\lambda_1 = 740$ nm and $\lambda_1 = 720$ nm shows the same trend (Figures S7 and S8, Supporting Information). This trend can be explained by the reactivity of formed macro-alkoxyamine after the fabrication of the bottom square. Similar to the reactivity of PA1 indicated by $1/P_{th}^2$ (shown in Figure 2a), macro-alkoxyamine has higher reactivity at 720 nm than at 740 nm and 760 nm. Surprisingly, one notices that for the same wavelength (λ_2) and power (P_2) for functionalization, the height of lines Δh on the top of a square made at $\lambda_1 = 760$ nm is larger

Table 1. Influence of laser powers P_1 and P_2 on the extent of polymerization Δh via NMP2.^{a)}

P_2	3.83 mW	6.08 mW	6.93 mW	7.95 mW	8.4 mW
P_1					
3.83 mW	$\Delta h = 267 \pm 25$ nm	$\Delta h = 380 \pm 18$ nm	$\Delta h = 469 \pm 21$ nm	$\Delta h = 528 \pm 17$ nm	$\Delta h = 554 \pm 23$ nm
5.14 mW	$\Delta h = 184 \pm 18$ nm	$\Delta h = 308 \pm 19$ nm	$\Delta h = 396 \pm 38$ nm	$\Delta h = 399 \pm 43$ nm	$\Delta h = 427 \pm 3$ nm
6.08 mW	$\Delta h = 73 \pm 32$ nm	$\Delta h = 182 \pm 18$ nm	$\Delta h = 221 \pm 6$ nm	$\Delta h = 278 \pm 17$ nm	$\Delta h = 306 \pm 27$ nm

^{a)} $\lambda_1 = \lambda_2 = 720$ nm.

Table 2. Summary of heights Δh obtained as a function of fabrication (λ_1) and functionalization (λ_2) wavelengths.

λ_2	720 nm	740 nm	760 nm
λ_1			
720 nm	$73 \leq \Delta h \leq 554$ nm	$34 \leq \Delta h \leq 522$ nm	$93 \leq \Delta h \leq 442$ nm
740 nm	$85 \leq \Delta h \leq 959$ nm	$25 \leq \Delta h \leq 914$ nm	$68 \leq \Delta h \leq 951$ nm
760 nm	$717 \leq \Delta h \leq 1203$ nm	$441 \leq \Delta h \leq 1161$ nm	$106 \leq \Delta h \leq 700$ nm

than the Δh on the top of a square made at $\lambda_1 = 740$ nm, and even further larger than for $\lambda_1 = 720$ nm. Here, all the bottom squares were made using a power close to the threshold, i.e., $P_1 = 3.83$ mW for $\lambda_1 = 720$ nm, $P_1 = 4.12$ mW for $\lambda_1 = 740$ nm and $P_1 = 6.25$ mW for $\lambda_1 = 760$ nm. Taking functionalization at $\lambda_2 = 720$ nm, $P_2 = 8.25$ mW as an example (Figure 3b; Figure S7, Supporting Information), the line's height Δh is 554 nm on the top of square made at $\lambda_1 = 720$ nm, while this value Δh is 959 nm on the top of square made at $\lambda_1 = 740$ nm and reaches 1203 nm at $\lambda_1 = 760$ nm. We assume that for a bottom square made at $\lambda_1 = 760$ nm, more macro-alkoxyamine is accessible. Finally, it has to be pointed out that the highest functionalization Δh is achieved at $\lambda_1 = 760$ nm and $\lambda_2 = 720$ nm. In Table 2, we list the ranges of heights that we can achieve at different fabrication (λ_1) and functionalization wavelengths (λ_2), which can serve as a guide to select the wavelength for surface functionalization.

Indeed, in our approach, by varying laser power and wavelength for fabrication and functionalization, the heights of functionalization can be tuned accurately from nano- to micro-scale, which is very important for surface functionalization applications.

2.3. Multi-Materials Fabrication via NMP2 3D DLW

Multi-material fabrication holds the innovation promise to integrate multiple materials, further combining different func-

tionalties into one object. As discussed above, NMP2 allows to introduce new monomers and new functionalities for surface modification, which establishes a solid foundation for the fabrication of multi-material microstructures. In order to explore the possibility of NMP2 in multi-material fabrication, several experiments were conducted.

2.3.1. Tunability of the Mechanical Properties

As shown in the top of Figure 4a, we used TMPTA or PEGDA (poly(ethyleneglycol)diacrylate) alone, without any photoinitiator, to write a micro-square onto a bottom square made from PETA + PA1 ($\lambda_1 = 760$ nm, $P_1 = 6.25$ mW), thanks to the presence of macro-alkoxyamine after the fabrication of the bottom square. Then, AFM-QNM was applied to measure the mechanical properties (Young's modulus) of the surface. Here, the TMPTA and PEGDA micro-squares were made at $\lambda_2 = 720$ nm, $P_2 = 6.8$ mW and the resulted heights are $0.61 (\pm 0.03)$ μm and $1.55 (\pm 0.07)$ μm , respectively. From AFM images (bottom of Figure 4a) and calculated Young's moduli, it is clear that these two micro-squares have different topography and mechanical properties (Young's modulus of 1.83 ± 0.022 GPa for TMPTA and 4.7 ± 0.4 MPa for PEGDA). This large difference of Young's modulus could be explained by the denser networks in TMPTA microstructures compared to that in PEGDA. Here, it is worth to point out that our approach can facily tune the mechanical properties of the surface over a wide range (from MPa to GPa, over 2 orders of magnitude). Furthermore, thanks to the living properties of NMP2, it gives the opportunity to modify the surface properties across multiple layers, which we will discuss in following.

2.3.2. Precise Successive Photoinduced Postmodification

To explore the living character of the microstructures, an IS2M logo was fabricated onto an assembly of two stacked

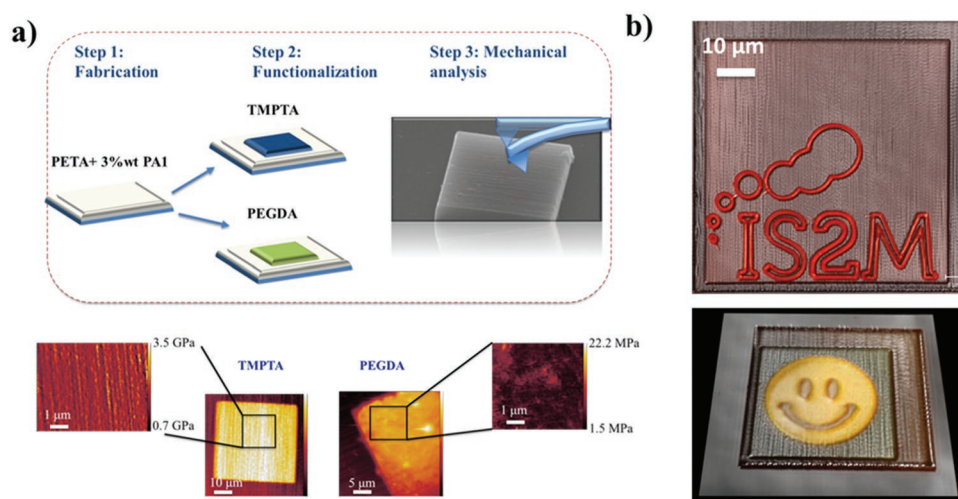


Figure 4. a) Post-modification and characterization of mechanical properties over 2 order of magnitude regarding the chosen monomer for functionalization (TMPTA or PEGDA). b) Customization and successive reconfigurations of surface properties of printed microstructures made by 3D DLW NMP2 and visualized by fluorescence and reflection confocal microscopies.

microstructures (Figure 4b top). Among these microstructures, the bottom square was made from PETA+PA1 using an excitation's wavelength $\lambda_1 = 760$ nm and a laser power $P_1 = 6.25$ mW. The subsequent square ($65 \mu\text{m} \times 65 \mu\text{m}$) and IS2M logo were fabricated from TMPTA with Rhodamine B (RB) at 760 nm (6.25 mW) and 720 nm (8.4 mW), respectively. Here, RB was added to visualize the functionalized part via confocal microscopy. One can notice that this IS2M logo has a well-defined shape and high resolution with smallest feature size (width) ≈ 520 nm. In order to further demonstrate the potential of our approach, one attractive pattern – a smiling face – was fabricated on the top of two squares. The experimental conditions are identical to the conditions for the IS2M logo on squares, except that here, the bottom square was made with RB in the formulation (i.e., PETA+PA1+RB), while no RB was used for the second square, in order to increase the contrast in confocal microscopy. Here, the smiling face has homogeneous height and well-defined shape, highlighted by the outline of eyes and mouth. These two exceptionally high-resolution microstructures clearly demonstrate the success of our approach in light-controlled surface modification. Remarkably, the surface modification and functionalization can be achieved successively. Moreover, living polymerization guarantees covalent linking between microstructures and their supporting surface.

Our approach, applying NMP2 for light-controlled surface modification, shows excellent results in modulating the

mechanical and chemical surface properties. Next, we will explore the potential of NMP2 in 3D and 4D printing.

2.3.3. Toward 4D Micro-Printed Objects

3D direct laser writing is a powerful tool to generate arbitrary microstructures. To demonstrate NMP2 in 3D printing, one Voronoi structure ($20 \mu\text{m} \times 20 \mu\text{m} \times 20 \mu\text{m}$) was achieved with a laser power $P_1 = 13.8$ mW at $\lambda_1 = 760$ nm. SEM images (Figure 5a,b) show that the structure is well-organized and has sub- μm resolution (≈ 450 nm). In addition, the hollow interior of the structures presents the good printability of PETA/PA1 resin and also proves that PA1 is an excellent photoinitiator.

The good printability of PETA/PA1 and the living property of NMP2 pave the way toward 4D printing. As defined by Skylar Tibbitts,^[20] 4D printing requires printed objects to be programmably active and to have the capability to transform independently over time off the print bed. Here, the introduction of living polymerization in 3D printing opens a door for 4D printing. As shown in Figure 5c, a cube was made by 3D DLW under irradiation at $\lambda_1 = 760$ nm, $P_1 = 6.25$ mW. Despite a little deformation of the cube due to the light penetration through a large object volume, the well-defined “4D NMP2” made at $\lambda_2 = 720$ nm and with $P_1 = 8.4$ mW (confocal microscopy image in Figure 5d) clearly demonstrate the exquisite spatial control in the surface modification of 3D microstructures.

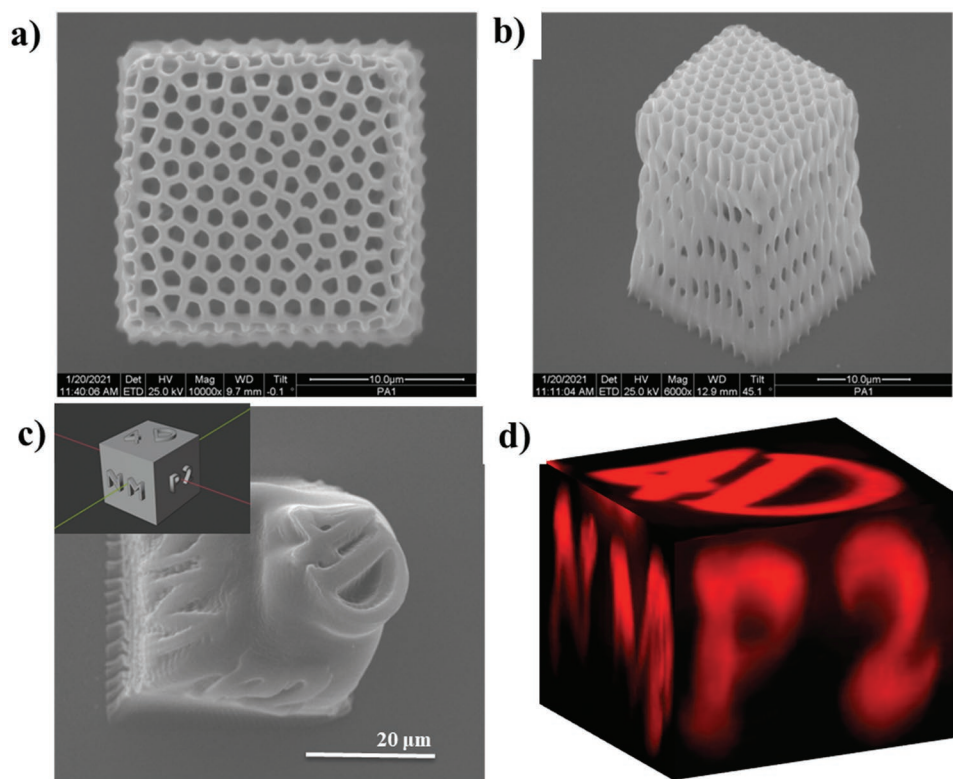


Figure 5. a) Top and b) tilted SEM images of Voronoi 3D microstructures ($\lambda_1 = 760$ nm, $P_1 = 13.8$ mW) c) CAD and SEM image combining fabrication of a cubic structure and its post-modification by “4D”, “NM” and “P2” letters on its faces. d) 3D fluorescence reconstruction imaging of the functionalized cubic structures with fluorescent TMPTA based formulation. Fabrication is performed at $\lambda_1 = 760$ nm, $P_1 = 6.25$ mW and functionalization is performed at $\lambda_2 = 720$ nm, $P_2 = 8.4$ mW.

3. Summary and Conclusion

In summary, we developed a new alkoxyamine based photore-sist compatible with 3D DLW to generate 4D microstructures. This 4D feature is provided by the living character of the printed 3D micro-objects, conferring them the ability to be customized on demand. To obtain this living materials, we exploited two-photon induced nitroxide mediated polymerization in 3D DLW to form reactive polymers during the 3D process. The two-photon polymerization efficiency of the alkoxyamine based resist has been demonstrated over a large range of wavelengths. Then, the influence of laser power and excitation wavelength for fabrication and post-modification experiments has been carefully investigated. It turns out that by playing on both parameters, a fine control of the photo-induced modification can be modulated from nano- to micrometer regimes. Taking advantage of these new insights, multi-material microstructures have been realized by performing successive reconfigurations of their surface properties. In particular, mechanical properties have been modulated over two order of magnitude and well-defined multi-chemistry patterns have been successfully produced thanks to the spatial and temporal control offered by the two-photon induced NMP2 post-modification. This work highlights new directions to be explored in order to accelerate the adoption of RDRP in 3D DLW and broadly speaking in 3D printing based on photopolymerization.

4. Experimental Section

Chemicals: Pentaerythritol triacrylate (PETA), Trimethylolpropane triacrylate (TMPTA), Poly(ethylene glycol) diacrylate (PEGDA, Mn = 700DA), Rhodamine B were purchased from Sigma-Aldrich and used as received. PA1 was synthesized according to the procedure described in Figure S2 (Supporting Information).

DLW Setup: The 3D microfabrication was carried out using a modified Microlight 3D printer based on a Zeiss Axio Observer D1 inverted microscope already described elsewhere.^[21] The two photon excitation was performed at 720, 740, or 760 nm using a mode-locked Ti:Sapphire oscillator (Chameleon Ultra II, Coherent: pulse duration: ≈140 fs; repetition rate: 80 MHz). The incident beam was focused with an objective lens (x40, NA: 0.65) into a drop of resist. The latter was deposited on a cover slip which was mounted on a XYZ piezoelectric stage allowing its translation relative to the laser focal point. This substrate was previously functionalized with 3-(triethoxysilyl)propyl methacrylate to enhance the adhesion of the structures onto the substrate. The generation of microstructures had been done via the computer-aided design (CAD) module of Simply.

Photostructuring: For fabrication experiments (Step 1), the resin was made from PETA and PA1 (3% wt.). It was stirred for 24 h to assure a good dissolution of the photoinitiator. For functionalization experiments (Step 2), the formulation was just TMPTA, PEGDA or TMPTA with a fluorophore (Rhodamine B). Typical procedure is as follow. A drop of the resin was deposited on a glass substrate and a square with an overlap of 0.3 μm was fabricated by 3D DLW. Once fabrication was done, the structure was washed with ethanol and dried. Then, a drop of monomer without initiator was deposited onto the square. Laser was then focused on the surface of the square for functionalization under controlled atmosphere (nitrogen). Sample was then washed with ethanol again to reveal the repolymerized structure. In all cases, the printing speed was set to 14.3 μm s⁻¹ for all squares, lines and other 2D and 3D microstructures (corresponding to an exposure time of 10 ms per voxel). Different laser intensities and wavelength had been used and are specified in the manuscript.

Scanning Electron Microscope (SEM): SEM images were obtained with a Quanta 400 FEI (Thermo Fischer Scientific). A thin gold layer of ≈15 nm was sputtered on samples before analysis.

Atomic Force Microscopy: Atomic Force Microscope (AFM) was used to investigate the morphology and mechanical properties of the microstructures. Young's modulus (according to either Derjaguin-Muller-Toporov (DMT) or Sneddon model) were measured using a Bruker Multimode 8 AFM in PeakForce Quantitative Nanomechanics (PeakForce QNM) mode. All images and profiles were treated and extracted using the Gwyddion software. QNM etched silicon probes were provided by Bruker and calibrated according to a procedure previously described.^[22]

Confocal Microscopy: Fluorescent and reflection images had been performed using a Zeiss Axio Imager M2 LSM 700 confocal right microscope controlled by ZEN 2012 software. A 405 nm laser diode was used as an excitation source to obtain the reflection of the materials, the detection was done with a photomultiplier (PMT). For fluorescence, excitation source was set at 488 nm and detection was performed on a PMT by suppressing the excitation light with a long pass filter (LP 491 nm). Acquisition was made with a 63x Oil "Apochromat Plan" objective lens (1.4 N.A. and working distance of 0.19 mm).

Statistical Analysis: 1. Pre-processing of data: AFM images were processed and analyzed with a software called Gwyddion. For the line heights measurements, it was necessary to set the 0 level on top of the square to only measure the proper line height. For that, the "three-point level" tool was used, which levels data by plane obtained by clicking on three points within data window. Outliers, which are clearly seen on the AFM images as their color was very bright, come from the degradation of the resin as the damage energy had been reached in those localized points. They can also be seen in the profiles drawn on top of the lines, which make it easier to remove them from the data. 2. Data presentation: The line heights are obtained using the "profile" tool, allowing the extraction of profiles along arbitrary lines from the image. Results presented are the means and standard deviation of each profile. 3. Sample size: A mean value of 125 points are measured across the line (depending on the outliers).

Supporting Information

Supporting Information is available from the Wiley Online Library or from the author.

Acknowledgements

The authors thank the Agence Nationale de la recherche (Project 2PhotonInsight ANR-16-CE08-0020-01, Project 3D CustomSurf ANR-19-CE06-0027, Project Mat-Light 4.0 ANR-21-EXES-0012) and Institut Carnot MICA for financial supports. This work was also partially supported by an Institutional Research Grant (MIPPI4D) from the Région Grand Est. The authors thank the members of MNMS axis for fruitful discussions and Stephan Knopf for helpful discussion regarding the scanning electron microscopy. KM thanks PHC Gilbert BioColor for funding.

Conflict of Interest

The authors declare no conflict of interest.

Data Availability Statement

The data that support the findings of this study are available from the corresponding author upon reasonable request.

Keywords

alkoxyamine, 3D direct laser writing, nitroxide-mediated photopolymerization, reversible deactivation radical polymerization, two-photon polymerization

Received: October 15, 2022

Revised: December 5, 2022

Published online:

- [1] a) A. Bagheri, K. E. Engel, C. W. A. Bainbridge, J. Xu, C. Boyer, J. Jin, *Polym. Chem.* **2020**, *11*, 641; b) V. A. Bobrin, J. Zhang, N. Corrigan, C. Boyer, *Adv. Mater. Technol.* **2022**, *n/a*, 2201054; c) K. Lee, N. Corrigan, C. Boyer, *Angew. Chem., Int. Ed.* **2021**, *60*, 8839; d) Z. Zhang, N. Corrigan, A. Bagheri, J. Jin, C. Boyer, *Angew. Chem., Int. Ed.* **2019**, *58*, 17954; e) B. J. Green, C. A. Guymon, *Addit. Manuf.* **2019**, *27*, 20; f) L. Qiao, M. Zhou, G. Shi, Z. Cui, X. Zhang, P. Fu, M. Liu, X. Qiao, Y. He, X. Pang, *J. Am. Chem. Soc.* **2022**, *144*, 9817.
- [2] a) M. Chen, Y. Gu, A. Singh, M. Zhong, A. M. Jordan, S. Biswas, L. T. J. Korley, A. C. Balazs, J. A. Johnson, *ACS Cent. Sci.* **2017**, *3*, 124; b) A. Bagheri, C. M. Fellows, C. Boyer, *Adv. Sci.* **2021**, *8*, 2003701; c) J. Cuthbert, A. Beziau, E. Gottlieb, L. Fu, R. Yuan, A. C. Balazs, T. Kowalewski, K. Matyjaszewski, *Macromolecules* **2018**, *51*, 3808.
- [3] A. Bagheri, C. W. A. Bainbridge, K. E. Engel, G. G. Qiao, J. Xu, C. Boyer, J. Jin, *ACS Appl. Polym. Mater.* **2020**, *2*, 782.
- [4] B. Zhao, J. Li, Z. Li, X. Lin, X. Pan, Z. Zhang, J. Zhu, *Macromolecules* **2022**, *55*, 7181.
- [5] A. Bagheri, H. Ling, C. W. A. Bainbridge, J. Jin, *ACS Appl. Polym. Mater.* **2021**, *3*, 2921.
- [6] M. Asadi-Eydivand, T. C. Brown, A. Bagheri, *ACS Appl. Polym. Mater.* **2022**, *4*, 4940.
- [7] a) C. Barner-Kowollik, M. Bastmeyer, E. Blasco, G. Delaittre, P. Müller, B. Richter, M. Wegener, *Angew. Chem., Int. Ed.* **2017**, *56*, 15828; b) S. Maruo, O. Nakamura, S. Kawata, *Opt. Lett.* **1997**, *22*, 132.
- [8] a) C. A. Koepele, M. Guix, C. Bi, G. Adam, D. J. Cappelleri, *Advanced Intelligent Systems* **2020**, *2*, 1900147; b) Q. Ji, J. Moughames, X. Chen, G. Fang, J. J. Huaroto, V. Laude, J. A. I. Martínez, G. Ulliac, C. Clévy, P. Lutz, K. Rabenoroso, V. Guelpa, A. Spangenberg, J. Liang, A. Mosset, M. Kadic, *Communications Materials* **2021**, *2*, 93; c) H. Ceylan, I. C. Yasa, M. Sitti, *Adv. Mater.* **2017**, *29*, 1605072.
- [9] a) A. S. Quick, J. Fischer, B. Richter, T. Pauloeuhl, V. Trouillet, M. Wegener, C. Barner-Kowollik, *Macromol. Rapid Commun.* **2013**, *34*, 335; b) B. Richter, T. Pauloeuhl, J. Kaschke, D. Fichtner, J. Fischer, A. M. Greiner, D. Wedlich, M. Wegener, G. Delaittre, C. Barner-Kowollik, M. Bastmeyer, *Adv. Mater.* **2013**, *25*, 6117.
- [10] a) M. Carlotti, V. Mattoli, *Small* **2019**, *15*, 1902687; b) D. W. Yee, M. D. Schulz, R. H. Grubbs, J. R. Greer, *Adv. Mater.* **2017**, *29*, 1605293; c) J. Zhang, H. Ding, X. Liu, H. Gu, M. Wei, X. Li, S. Liu, S. Li, X. Du, Z. Gu, *Small* **2021**, *17*, 2101048.
- [11] X. Wu, B. Gross, B. Leuschel, K. Mougín, S. Dominici, S. Gree, M. Belqat, V. Tkachenko, B. Cabannes-Boué, A. Chemtob, J. Poly, A. Spangenberg, *Adv. Funct. Mater.* **2022**, *32*, 2109446.
- [12] Y. Jia, C. A. Spiegel, A. Welle, S. Heißler, E. Sedghamiz, M. Liu, W. Wenzel, M. Hackner, J. P. Spatz, M. Tsotsalas, E. Blasco, *Adv. Funct. Mater.* **2022**, *n/a*, 2207826.
- [13] a) Y. Guillauneuf, D. Bertin, D. Gigmes, D.-L. Versace, J. Lalevée, J.-P. Fouassier, *Macromolecules* **2010**, *43*, 2204; b) D. L. Versace, J. Lalevée, J. P. Fouassier, Y. Guillauneuf, D. Bertin, D. Gigmes, *Macromol. Rapid Commun.* **2010**, *31*, 1383.
- [14] a) Y. Guillauneuf, D.-L. Versace, D. Bertin, J. Lalevée, D. Gigmes, J.-P. Fouassier, *Macromol. Rapid Commun.* **2010**, *31*, 1909; b) S. Telitel, S. Telitel, J. Bosson, A. Spangenberg, J. Lalevée, F. Morlet-Savary, J.-L. Clément, Y. Guillauneuf, D. Gigmes, O. Soppera, *Adv. Mater. Interfaces* **2014**, *1*, 1400067.
- [15] S. Telitel, J. C. Morris, Y. Guillauneuf, J.-L. Clément, F. Morlet-Savary, A. Spangenberg, J.-P. Malval, J. Lalevée, D. Gigmes, O. Soppera, *ACS Appl. Mater. Interfaces* **2020**, *12*, 30779.
- [16] M. Baron, J. C. Morris, S. Telitel, J.-L. Clément, J. Lalevée, F. Morlet-Savary, A. Spangenberg, J.-P. Malval, O. Soppera, D. Gigmes, Y. Guillauneuf, *J. Am. Chem. Soc.* **2018**, *140*, 3339.
- [17] R. B. Grubbs, J. K. Wegrzyn, Q. Xia, *Chem. Commun.* **2005**, *1*, 80.
- [18] T. Baldacchini, C. N. LaFratta, R. A. Farrer, M. C. Teich, B. E. A. Saleh, M. J. Naughton, J. T. Fourkas, *J. Appl. Phys.* **2004**, *95*, 6072.
- [19] M. Nardi, E. Blasco, C. Barner-Kowollik, *J. Am. Chem. Soc.* **2022**, *144*, 1094.
- [20] S. Tibbits, *Architectural Design* **2014**, *84*, 116.
- [21] S.-Y. Yu, G. Schrodj, K. Mougín, J. Dentzer, J.-P. Malval, H.-W. Zan, O. Soppera, A. Spangenberg, *Adv. Mater.* **2018**, *30*, 1805093.
- [22] M. Belqat, X. Wu, L. P. C. Gomez, J.-P. Malval, S. Dominici, B. Leuschel, A. Spangenberg, K. Mougín, *Addit. Manuf.* **2021**, *47*, 102232.